UNIVERSITÀ DEGLI STUDI DI TRIESTE

UNIVERSITÀ DEGLI STUDI DI TRIESTE

XXXIV CICLO DEL DOTTORATO DI RICERCA IN

SCIENZE DELLA RIPRODUZIONE E DELLO SVILUPPO

CORRELATION BETWEEN TISSUE ABNORMALITIES AND MYOCARDIAL DEFORMATION INDICES IN ARRHYTHMOGENIC CARDIOMYOPATHY: A MULTIMODALITY IMAGING STUDY

Settore scientifico-disciplinare: **MED11**

DOTTORANDO
DR. ANTONIO DE LUCA

COORDINATORE
PROF. PAOLO GASPARINI

SUPERVISORE DI TESI
PROF. MARCO MERLO

ANNO ACCADEMICO 2020/2021

TABLE OF CONTENTS

ABSTRACT

AIMS. Speckle Tracking Echocardiography (STE) and Feature Tracking Cardiac Magnetic Resonance imaging (FT-CMR) are advanced imaging techniques which are increasingly used for the quantification of myocardial deformation indices. We aimed to study the diagnostic performance of biventricular strain parameters provided by STE and FT-CMR and to evaluate their correlation with tissue abnormalities in patients with definite diagnosis of arrhythmogenic cardiomyopathy (AC).

METHODS. 41 AC Patients with available echocardiography (ECHO) and CMR study along with 41 healthy subjects who underwent complete ECHO study and 41 healthy subjects who underwent CMR scan were enrolled. Myocardial deformation indices (i.e. global longitudinal strain -GLS-; global circumferential strain -GCS-; global radial strain -GRS-) for both ventricles were calculated using STE and FT-CMR analysis. Quantification of tissue abnormalities (i.e. fat and late gadolinium enhancement -LGE- extension) was performed.

RESULTS. All left and right ventricular (LV and RV) strain parameters were significantly impaired in AC patients compared with healthy subjects for both STE and FT-CMR analysis. There was a good correlation between ECHO LV GLS and both CMR LV 3DGLS and LV 2DGLS (Spearman's Rho [r_s] = 0.662, $p < 0.001$ and 0.561, $p < 0.001$ respectively). All myocardial deformation indices, in particular GLS, were moderately associated with LGE extension (ECHO LV GLS $r_s = 0.461$, $p = 0.008$; ECHO RV GLS 0.506, $p = 0.003$; CMR LV 3DGLS $r_s = 0.423$, $p = 0.016$; CMR RV 2DGLS $r_s = 0.385$, $p = 0.030$). The accuracy in diagnosing AC of both techniques was overall good (area under the receiver-operating characteristics curve -AUC- for ECHO LV GLS = 0.862; ECHO RV GLS AUC = 0.852; CMR LV 2DGLS AUC = 0.844; CMR RV 2DGLS AUC = 0.778).

CONCLUSIONS. All myocardial deformation indices were impaired in AC patients compared to healthy subjects and were significantly associated with the extension of CMR tissue abnormalities. Strain analysis by STE and FT-CMR, mostly GLS, showed a good diagnostic performance in identifying the disease and should be implemented in diagnostic algorithms.

INTRODUCTION

Arrhythmogenic Cardiomyopathy (AC) is a genetically determined myocardial disorder, characterized by progressive cardiomyocyte loss and fibro-fatty replacement [1,2]. Electrical instability and ventricular dysfunction are essential aspects of the disease, clinically translating into the occurrence of hyperkinetic scar-related ventricular arrhythmias, sudden cardiac death (SCD) and heart failure (HF) [3].

In the pre-genetic and pre-cardiac magnetic resonance (CMR) era, AC has been regarded as a predominantly right ventricular (RV) disease. More recently, the spread of CMR together with genotype-phenotype correlation studies led to an increasing awareness of the frequent left ventricular (LV) involvement [4,5], characterized by an increased risk of events such as death, HF, heart transplantation (HT) and major ventricular arrhythmias [6,7]. In a recent study, LV histopathologic involvement was detected in 87% of 202 AC subjects, with isolated LV disease in 17% of cases [8].

Nowadays, the diagnosis of AC is based on International Criteria according to a scoring system that considers clinical and pathological features of the disease, grouped into 6 categories (i.e. global or regional dysfunction and structural abnormalities; histological tissue characterization; ECG repolarization abnormalities; ECG depolarization/conduction abnormalities; arrhythmias; family history and genetics) [1]. Definite diagnosis requires 2 major criteria, or 1 major and 2 minor criteria, or 4 minor criteria from different categories. However, these criteria apply only to the classical RV form, not considering the broader spectrum of the disease phenotypes.

Recently, an International Expert Consensus document [9] proposed an upgrade of the diagnostic criteria, taking into account the left-side involvement and introducing tissue characterization by CMR as a landmark point. The document also considered the demonstration of reduced LV global longitudinal strain (GLS) as minor morpho-functional criterion for the diagnosis of biventricular and left-dominant (LD) variants, highlighting its ability to unmask subtle changes, particularly relevant in early stages of the disease [10, 11]. In fact, standard volumetric techniques have several limitations in the detection of the initial impairment of ventricular systolic function. Conversely, deformation imaging allows a precise quantification of cardiac mechanics by directly evaluating myocardial fiber deformation.

Speckle tracking echocardiography (STE) showed to be able to detect subtle alterations in myocardial function in several pathological conditions [12]. However, this technique is strictly dependent on image quality. Feature Tracking Cardiac Magnetic Resonance (FT-CMR) study has emerged as alternative to 2D-echocardiography for the whole strain analysis (i.e. 2D/3D GLS, global circumferential strain -GCS- and global radial strain -GRS), highly reproducible and independent of the echocardiographic acoustic window [13].

In the setting of AC, recent studies suggested the ability of deformation imaging to detect the disease, to predict its progression and to stratify the risk of major cardiac events [14,15,16,17,18]. However, limited evidence is available about the role of deformation imaging in identifying LV involvement [19]. Likewise, direct comparisons of STE and FT-CMR analysis in AC are limited [20]. Moreover, the correlation between impairment of biventricular strain parameters and the extension of tissue abnormalities by CMR was not previously explored.

Thus, the aim of the present study was to evaluate the diagnostic utility of deformation imaging parameters provided by STE and FT-CMR and their correlation with the extension of tissue abnormalities in a cohort of AC patients.

METHODS

Study population

AC patients consecutively enrolled in the Trieste Heart Muscle Disease Registry (HMDR) from January 1st, 2008 to December 31st, 2020 with available transthoracic echocardiography examination and CMR scan within 6 months of each other were included in the present analysis. Patients with inadequate image quality for STE analysis and patients with unstable heart rhythm were excluded.

All patients fulfilled the diagnostic criteria for “definite ARVC” according to 2010 Revised Task Force Criteria [1]. Data regarding patients enrolled before 2010 were carefully revised to confirm the diagnosis.

Patients were classified into three phenotypic subgroups according to ventricular involvement: (I) lone RV AC, if an isolated RV involvement at echocardiography and/or CMR evaluation was documented. RV involvement was defined as the presence of regional wall motion abnormalities -WMA- (akinesia, dyskinesia or aneurism), in association with RV dilatation and/or global RV systolic dysfunction (according to the imaging test specific nomograms) [1]; tissue abnormalities by CMR were also considered [9]. (II) Biventricular AC, if an involvement of both ventricles (i.e. WMA, systolic dysfunction and tissue abnormalities) was documented at echocardiography and/or CMR. (III) LD AC, if an isolated LV involvement was documented at echocardiography and/or CMR. LV involvement was defined by the presence of LV WMA, global LV systolic dysfunction (according to the imaging test specific nomograms) with or without LV dilatation; tissue abnormalities by CMR were also considered [9].

Endomyocardial biopsy was performed in 2 patients (1 familial, 1 sporadic) with LD form in order to exclude an inflammatory disease and confirm the diagnosis.

Patients were compared with a sample of healthy volunteers who underwent complete transthoracic echocardiography and CMR scan at our Center.

All data were anonymized and entered into an Excel-based datasheet.

All patients provided written informed consent for enrollment in the Registry. The study was approved by the institutional review board and complies with the Declaration of Helsinki.

Echocardiography

A comprehensive transthoracic echocardiography was performed with 2D, color and Doppler imaging, using Vivid E9, Vivid E95 (GE Healthcare, Little Chalfont, UK) or iE33 (Phillips Medical Systems, Andover, MA, USA) ultrasound systems. Image analysis was conducted according to international guidelines [21,22]. Using a vendor-independent software (TomTec-Arena 5.4, Munich, Germany), STE analysis was performed in order to obtain LV peak GLS, GCS, GRS, RV GLS and RV free wall longitudinal strain -FWLS-, according to international recommendations [23,24]. LV and RV focused views with a frame rate ≥50 fps were used. In particular, LV apical two-, three-, and four-chamber views were used for the

quantification of LV-GLS. Parasternal short-axis view at the level of papillary muscles was used for the quantification of LV GCS and GRS. RV GLS and FWLS were measured from RV focused apical view. After tracing of the endocardial borders, the software automatically tracked speckles throughout the cardiac cycle, deriving strain parameters. End-diastole and end-systole were defined by both electrocardiogram and visual assessment of 2D images. In case of suboptimal tracking, contours were manually corrected and analysis repeated. Inter- and intra-observer variability of our Center for speckle tracking analysis were previously reported [25,26].

CMR acquisition protocol

CMR studies were performed on 1.5 or 3 Tesla Magnetic Resonance scanners (Philips Intera, Philips Ingenia) with a cardiac phased-array receiver surface coil, ECG-gating and breath-hold technique, using a dedicated cardiac software. Cine images in two-, three- and four-chamber views, a stack of contiguous short-axis slices from the atrioventricular plane to the apex and para-axial slices from diaphragm to the entire outflow were acquired using a steady-state free precession (SSFP) pulse sequence (temporal resolution ≤50 ms; spatial resolution with a mean acquisition pixel size of 1.6×1.6 mm; slice thickness = 8 mm, no inter-slice gap; repetition time/echo time = 3.0/1.5 ms). T1- or proton density-weighted turbo spin-echo (TSE) pulse sequences were acquired using the same slice coverage as cine images. Approximately 10 minutes after intravenous administration of 0.1-0.2 mmol/kg gadolinium-based contrast agent late gadolinium enhancement (LGE) images were acquired in the same views using segmented T1-weighted inversion-recovery prepared gradient-echo or phase sensitive inversion recovery (PSIR) pulse sequences, individually adjusting inversion time to optimize nulling of apparently normal myocardium.

CMR image analysis

CMR studies were analyzed offline using a dedicated software (Circle CVI-42, Circle Cardiovascular Imaging, Calgary, Canada). LV and RV volumes and function were measured using the standard volumetric technique from the cine short axis stack, with the endocardial border traced at end-diastole and end-

systole for each slice and the epicardial border traced at end-diastole [27]. Volume and mass measures were indexed to body surface area. In SSFP images, intramyocardial fat was detected as a hyperintense region bordered by a thin hypointense boundary and surrounded by normal myocardium ("India Ink" artifact). Presence of intramyocardial fat was confirmed by the detection of hyperintense signal in TSE images in the same anatomical location. Extent of intramyocardial fat was measured in SSFP images by a manual contouring of "India Ink" artifact and expressed as percentage of total ventricular myocardial area [28]. LV and RV wall motion were assessed with a visual scoring system in which 1 = normal, 2 = hypokinetic, 3 = akinetic, 4 = dyskinetic, 5= aneurysm. For LV a 17-segment model was used [29]. For RV, in the absence of standardization, a 5-segment model was arbitrarily used (RV lateral basal, RV lateral mid portion, RV apex, RV inferior, RV outflow tract). Wall motion score index (WMSI) for both ventricles was calculated as the cumulative sum of individual segment scores divided by the number of interpreted segments.

Post-contrast images were evaluated for the presence of LGE, defined as areas with increased signal intensity following administration of contrast medium in two orthogonal planes. In the absence of consensus regarding the technique of quantification, the extent of LV LGE was quantified by measuring regions with signal intensity >6 standard deviations above nulled remote myocardium. Manual correction was performed for obvious threshold errors. The extent of LGE was expressed as percentage of total LV mass [30]. Similarly, in the absence of dedicated software tool and standardized method, RV LGE was quantified by manual contouring of hyperintense areas of RV walls and expressed as percentage of total RV myocardial area.

FT-CMR analysis was performed on SSFP images using a dedicated tool that allows the quantification of LV and RV strain values. After uploading the short- and long-axis images (2-chamber, 3-chamber and 4-chamber views), the brightness was optimized to ensure optimal endocardial/blood pool discrimination. The endocardial and epicardial borders were manually traced on the end-diastolic frame. The software automatically tracked the contours throughout the full cardiac cycle. Contours were manually adjusted and analysis repeated in case of suboptimal tracking. Biventricular strain parameters (2D and 3D GLS, GCS and GRS for LV; 2D GLS, GCS and GRS for RV) were automatically generated. GLS was

derived from the peak systolic strain values of segments in the longitudinal view. The GCS and LV GRS were obtained from the peak strain values of the segments in short-axis sections. For RV, GRS was evaluated in long axis images. Inter- and intra-observer variability of our Center for feature tracking analysis were previously reported [26].

Study purposes

The aims of the present study were:

1. to compare myocardial deformation indices derived from STE and FT-CMR in AC patients;
2. to evaluate the myocardial deformation indices by STE and FT-CMR in AC patients, compared with healthy controls;
3. to evaluate the correlation between strain parameters measured by STE and FT-CMR and the extension of tissue abnormalities detected through CMR imaging;
4. to evaluate the diagnostic performance of STE and FT-CMR and to identify diagnostic cutoffs for the discrimination between healthy and disease affected-subjects.

Statistical analysis

Summary statistics of clinical and instrumental continuous variables were expressed as mean and standard deviation or median and interquartile range as appropriate. Categorical data are presented as absolute numbers and percentages. The χ^2 test (for categorical variables) was used to determine differences between two groups. Comparisons of means for normally distributed variables were performed by analysis of variance (ANOVA) with the Bonferroni post-hoc correction for multiple comparisons. For non-normally distributed variables, the Kruskal–Wallis test (multiple groups) and Mann–Whitney U-test (two groups) were used. Sample size was based on the hypothesis that the correlation coefficient was 0.50. 30 patients were required for this correlation coefficient to be significantly different from 0, with an α-level of 0.05 and for a β-level of 0.20 (power is 80%). Considering that possible technical problems in reading the values from images could happen, the sample size was increased to enroll 41 patients. The non-parametric Spearman rank correlation coefficient (Spearman's rho, r_s) was used to

assess linear correlations between myocardial deformation indices and tissue abnormalities. Receiver-Operating Characteristic (ROC) analysis was used to evaluate the accuracy of strain analysis in detecting affected subjects, with an area under the curve (AUC) value of 0.50 indicating no accuracy and a value of 1.00 indicating maximal accuracy. Optimal cutoff points as provided by Youden index were chosen as reference points and further adapted.

Analyses were carried out using IBM SPSS Statistics software version 28.

RESULTS

Study population

Forty-one patients fulfilling inclusion criteria were enrolled in the present study, along with 41 healthy subjects who underwent complete echocardiography and 41 healthy subjects who underwent CMR scan. Table 1 summarizes characteristics of the study population. Mean age was 44 ± 13 years and 26 (63%) were men. Eight (20%) patients had a lone RV AC, 24 (58%) presented a biventricular AC and 9 (22%) had a LD AC. Patients with LD AC were significantly younger than biventricular AC subgroup.

Common CMR parameters are presented in the Table 2. Mean LV end-diastolic volume index (EDVi) was 94 ± 26 ml/m^2 and mean LV ejection fraction (EF) was 54 ± 10%. There was not significant difference in LV EDVi and LVEF according to AC phenotype. Mean RV EDVi was 107 ± 32 ml/m^2, with larger volumes in lone RV subgroup. Mean RVEF was 49 ± 12%, with significantly lower RVEF in lone RV and biventricular forms. Twenty-five (57%) patients showed LV fat infiltration and 27 (61%) LV LGE, with significantly higher prevalence in biventricular and LD forms. Twenty-four (54%) and 14 (32%) showed RV fat infiltration and RV LGE respectively. Patients with biventricular AC presented larger fat extension for both ventricles when compared to the other subgroups (LV fat extension 1.61% of LV mass, IQR 0.29-2.91; RV fat extension 4.33% of RV mass, IQR 2.07-10.85), whereas LD forms presented highest LV LGE extension (13.35% of LV mass, IQR 8.60-24.07).

All LV and RV strain parameters, for both echocardiography and CMR, were significantly impaired in patients when compared with controls (Table 3). There was no significant difference in LV strain

parameters according to AC phenotypes for both STE and FT-CMR (Table 4). Conversely, echocardiographic RV GLS and FWLS were significantly more impaired in biventricular and lone RV AC compared to those with LD AC (RV GLS -14.72±5.48 in biventricular AC *vs*. -17.48±3.88 in lone RV AC and -21.29±4.76 in LD AC, p = 0.007; RV FWLS -14.92±6.38 *vs*. -16.82±4.96 *vs*. -22.17±4.67 respectively, p = 0.011). Biventricular and lone RV forms showed more impaired CMR 2D RVGRS when compared with LD AC (33.91±19.67 *vs*. 44.22±9.44 *vs*. 57.30±20.73 respectively, p = 0.007). A trend towards lower CMR 2D RVGLS was also observed.

Correlations between STE and FT-CMR analysis

Table 5 reports correlations between STE and FT-CMR analysis. There was a strong association between echocardiographic LV GLS and CMR LV 3DGLS (r_s = 0.662, p < 0.001) and moderate association between LV GLS and CMR LV 2DGLS (r_s = 0.561, p < 0.001) (Figure 1). There was also a moderate association between echocardiographic LV GRS and CMR 2D/3D GRS (r_s = 0.409 and 0.423, p = 0.042 and p = 0.035 respectively), however with a wide dispersion (Figure 2). There was no significant correlation between echocardiographic RV GLS and CMR RV 2DGLS (p = 0.084).

Correlations between STE and CMR parameters of biventricular involvement

Table 6 reports the correlations between STE analysis and CMR indices of LV and RV involvement. LV GLS was strongly associated with LV WMSI (r_s = 0.683, p < 0.001). Similarly, there was a strong association between either RV GLS and RV FWLS with RV WMSI (r_s = 0.706 and 0.686 respectively, p < 0.001).

We found a moderate association between LV GLS and LV LGE extension (r_s = 0.461, p = 0.008). RV strain parameters were moderately associated with RV LGE extension (r_s for RV GLS = 0.506, p = 0.003; r_s for RV FWLS = 0.484, p = 0.005). There was also a moderate association between RV GLS and RV fat extension (r_s = 0.433, p = 0.013).

Figures 3 and 4 show the correlation between LV and RV GLS with LGE extension. Interestingly, a significant proportion of patients presented a compromised GLS despite a normal post-contrast signal (i.e. LGE 0%).

Correlations between FT-CMR analysis and other CMR parameters of biventricular involvement

Table 7 reports the correlations between FT-CMR analysis and other CMR indices of LV and RV involvement. All LV strain parameters were strongly associated to LV WMSI, whereas RV strain parameters were moderately associated with the extension of RV WMA. Focusing on LV, there was a moderate association between 3DGLS and LGE extension (r_s = 0.423, p = 0.016) and between 2D GRS and LGE extension (r_s = -0.417, p = 0.018). 2D/3D GCS and 3D GRS were only weakly associated with LGE extension. About RV, all strain parameters were moderately associated with LGE extension. None of strain parameters, neither LV nor RV, were associated with fat extension. Similar to STE, also FT-CMR analysis showed a significant impairment of myocardial deformation indices of both ventricles in a significant proportion of patients without any evidence of tissue abnormalities (Figures 5 and 6).

Diagnostic performance analysis of STE

Figure 7 shows the ROC curves describing the diagnostic performance of echocardiographic strain parameters for distinction between patients affected by AC and healthy subjects. As reported in Table 8a, the diagnostic accuracy as quantified by the area under the receiver-operating characteristics curve (AUC) was highest for LV GLS (AUC = 0.862; 95% CI 0.778-0.945), RV GLS (AUC = 0.852; 95% CI 0.766-0.938) and RV FWLS (AUS = 0.822; 95% CI 0.726-0.918). The derived best cutoff values were -20.35 for LV GLS, -20.45 for RV GLS and -20.05 for RV FWLS.

Diagnostic performance analysis of FT-CMR

Figure 8 shows the ROC curves describing the diagnostic performance of CMR strain parameters for distinction between patients affected by AC and healthy subjects. As reported in Table 8b, the AUC

was excellent for 2D LVGLS (AUC = 0.844; 95% CI 0.759-0.930), 2D LVGRS (AUC = 0.825; 95% CI 0.735-0.914), 3D LVGRS (AUC = 0.817; 95% CI 0.723-0.910) and 2D RVGCS (AUC = 0.839; 95% CI 0.749-0.929). AUC was acceptable for all other CMR strain parameters (all > 0.7). Among others, the derived best cutoff values were -19.92 for LV 2DGLS, -24.6 for RV 2DGLS and -12.95 for RV 2DGCS.

DISCUSSION

Main findings

To the best of our knowledge, the current study is the first one that evaluates comprehensively the role of myocardial deformation imaging provided by STE and FT-CMR in a well characterized cohort of definite AC (Central illustration). Specifically, the results of our research can be summarized as follows: (1) patients with AC have impaired LV and RV strain parameters compared with healthy controls, for both STE and CMR-FT; (2) a moderate association between deformation indices provided by STE and FT-CMR analysis and LGE extension for both ventricles has been demonstrated; (3) there is a moderate association between STE and FT-CMR analysis, in particular for LV GLS; (4) both STE and FT-CMR analysis showed high diagnostic accuracy, in particular again for GLS.

Myocardial deformation imaging for the diagnosis of arrhythmogenic cardiomyopathy

Despite the advances of the last decade in management of the disease, the diagnosis of AC remains challenging. Indeed, the lack of a single conclusive test leads to a mandatory multiparametric evaluation. According to international Task Force criteria (TFC) [1], definition by imaging modalities relies on the presence of RV dilatation, dysfunction and regional wall motion abnormalities (WMA). However, the evaluation of the RV remains a significant issue due to its complex geometry, fiber orientation, contraction pattern and thin myocardial wall [31]. Furthermore, the assessment of regional WMA may be difficult, even for experienced operators. In this setting deformation imaging could be a useful tool for a more sensitive and objective evaluation of ventricular mechanics, particularly in the early stages and in subjects at risk for developing the disease such as genetic mutation carriers [14,17]. Moreover, TFC focused on RV disease manifestations, not considering the frequent LV involvement [1]. Of note, the latter may be

missed by conventional imaging, especially when subclinical involvement is present. In fact, even in the absence of LV WMA, extensive tissue anomalies can be detected by CMR. We found a good diagnostic accuracy of strain analysis provided by both STE and FT-CMR in identifying the disease, mainly through the most studied of these parameters, the GLS. These results confirm and expand the current knowledge [15,16,19,32,33,34] and suggest the complementary use of STE and FT-CMR in the diagnostic process, particularly in morpho-functionally normal phenotypes, on top of tissue characterization.

Evaluation of right ventricular involvement

In our study, patients with AC showed a significantly impaired RV strain by both STE and FT-CMR, compared to controls. This finding confirms previous observations. In a series by Prati et al. RV GLS, GCS and GRS were all significantly lower among patients with ARVC compared with those with RV outflow tract arrhythmias and healthy controls. The authors concluded that FT-CMR analysis helps to objectively quantify global and regional RV dysfunction and provides incremental value over conventional cine CMR imaging [15]. In another study by Heermann et al. RV global longitudinal strain rate was significantly reduced in definite and borderline ARVC patients in comparison with healthy volunteers. Interestingly, this parameter was significantly reduced even in patients with normal RVEF [35]. Of note, the accuracy of strain analysis in detecting RV forms was demonstrated across a wide spectrum of clinical scenarios, ranging from adolescents to athletes and other arrhythmogenic conditions [16,32,33].

Evaluation of left ventricular involvement

Although AC was historically considered a RV disease, more recently a frequent LV involvement was recognized and associated with worse outcomes [6,7,36]. A recent International Expert Consensus document [9] proposed new criteria for the diagnosis of isolated LV form of AC, considering the presence of global LV systolic dysfunction with or without dilatation, regional WMA and presence of epicardial or midmyocardial LGE. However, limited data are available on deformation imaging in this field. In a study by Mast et al. [37] echocardiographic deformation imaging detected a higher incidence of LV involvement compared with conventional echocardiography in patients with ARVC and pathogenic mutation–positive

relatives. Moreover, LV involvement detected by deformation imaging was an independent predictor of major events during approximately 6 years follow-up. In another study by Chen et al., LV involvement was evaluated in 68 ARVC patients through FT-CMR [34]. Compared with controls, LV global and regional longitudinal, circumferential and radial strain were all significantly impaired in patients with reduced LVEF, whereas only LV GLS as well as mid and apical longitudinal peak strain were significantly reduced in preserved LVEF subgroup. Similar findings were reported by Shen et al. [19], who described a significant impairment of all LV strain parameters, even in patients with preserved LVEF. In that study, LV GLS >−12.65% was an independent predictor of adverse cardiac outcomes during a mean follow-up period of 4 years. Our results are consistent with previous observations and supports the frequent LV involvement in AC detected by both STE and FT-CMR analysis. Interestingly, LV strain parameters were all impaired across the entire phenotypic spectrum of the disease, without significant difference between lone RV, biventricular and LD AC subgroups. It could be hypothesized that an abnormal deformation unmasked by strain imaging reflects a diffuse impairment of mechanical contraction proprieties of the heart as expression of the genetic substrate of the disease. In fact, it is wildly accepted that desmosomal gene mutations are responsible of disruption of mechanical linkage between cells in response to stress, leading to cardiomyocyte loss and fibro-fatty replacement [38]. Deformation imaging could intercept these mechanisms affecting the entire myocardium, revealing a true biventricular disease.

Myocardial deformation indices and tissue abnormalities

Previous observations reported an association between the presence of LGE and the impairment of LV deformation indices in small series [37,34]. Mast et al. described a good correlation between location of LGE and LV segments showing an abnormal regional deformation in group of 4 patients, with better agreement than visual wall motion analysis [37]. At the same time, they reported a LV involvement according to deformation imaging also in 9 patients without any evidence of LGE. Similarly, Chen et al. found that the LV segments with LGE showed impaired LV peak strain in all directions compared to those without LGE [34]. Moreover, radial strain was significantly reduced in LGE-positive segments in the

subgroup with preserved LVEF. To our knowledge, we described for the first time a significant association between echocardiographic GLS and LGE extension, as well as FT-CMR strain parameters and LGE extension. Interestingly, a significant proportion of patients showed compromised myocardial deformation indices of both ventricles without any evidence of macroscopic tissue abnormalities. This observation again supports the hypothesis that deformation imaging can detect also minor abnormalities in myocardial mechanics and could reflect the presence of microscopic fibrosis and/or scars not identified by LGE technique. This concept is supported by previous evidences that described only poor agreement between LGE and electroanatomic mapping to detect myocardial scar as arrhythmogenic substrate [39,40]. As already reported, circumferential strain was significantly impaired in segments with dense scar at electroanatomic mapping [40]. Furthermore, lower strain was associated with endocardial and epicardial dense scar as well as ventricular tachycardia culprit sites [40]. Further studies exploring the potential role of new CMR techniques such as T1-mapping and extracellular volume (ECV) quantification would be advisable in this field.

Comparison between STE and FT-CMR imaging

Evidence regarding the relationship between STE and FT-CMR analysis are currently limited. In a recent study, Taha et al. performed a head-to-head comparison between the two techniques for the assessment of RV deformation [20]. Authors reported a significant correlation between RV strain values. However, agreement between techniques was weak. Moreover, both correlation and agreement decreased when regional strain were analyzed. In our study we described a moderate correlation between LV strain parameters, in particular LV GLS provided by STE and FT-CMR in definite AC. Conversely, we did not find a significant correlation between RV GLS and RV 2DGLS measured by FT-CMR. These findings support the recommendation that values obtained by these techniques cannot be used interchangeably in clinical practice [20].

In light of these results, we strongly recommend the extensive use of STE analysis as first line investigation for the diagnosis of AC and in particular to detect the LV involvement, that needs to be

confirmed by CMR imaging. Moreover, the addition of strain analysis to conventional CMR evaluation could be useful to identify also minor biventricular abnormalities. Similarly, STE analysis should be systematically performed at the time of family members' screening evaluation, in order to detect early signs of the disease and potentially guiding the indication to perform or repeat CMR. Future studies on larger populations are needed to clarify the prognostic implications of these findings.

LIMITATIONS

Some limitations need to be acknowledged. First of all, the small size of our study cohort might limit the impact of our observations. However, as far as we know this is the first study investigating the association between the extension of tissue abnormalities and the impairment of myocardial deformation indices in AC. Moreover, the sample size was calculated to have an adequate statistical power. We consider our findings to be hypothesis generating. These preliminary results need to be confirmed in larger series. Furthermore, studies on larger populations are needed to elucidate the prognostic implications of biventricular myocardial deformation analysis in AC.

Secondly, echocardiography and CMR were not performed at the same time. However, although AC is considered a progressive disease, it is unlikely to observe a significant progression over 6 months period [17,41].

Biventricular fat extension as well as RV LGE was manually quantified. However, dedicated software tools are not still available.

Parasternal short-axis view at the level of papillary muscles was used for echocardiographic LV GCR and GRS calculation and assumed as representative of the global deformation of the LV in these directions, as already proposed by other research groups [42]. In our opinion this specific view is the best for STE analysis in the short-axis plane as it generally avoids geometric distortions.

Genetic data and genotype-phenotype correlations were not explored in the present study.

CMR control group was significantly younger than AC patients. However, despite statistically significant, this difference was clinically negligible. In fact, it was demonstrated that the effect of age on deformation indices becomes relevant in older subjects [43,44,45].

Lastly, given the impairment of myocardial deformation indices in the absence of macroscopic tissue abnormalities in a significant proportion of patients, it would be interesting to explore the association with microscopic fibrosis. However, T1-mapping and ECV calculation was not available due to the retrospective design of the study.

CONCLUSIONS

Myocardial deformation indices of both ventricles are significantly impaired in patients affected by AC. Moreover, impairment of strain parameters is significantly associated with extension of tissue abnormalities detected by CMR. Strain analysis, in particular GLS, shows a good diagnostic performance in identifying the disease and should be implemented in diagnostic algorithms. Further studies are needed to validate these observations, to analyze genotype-phenotype correlations and to explore the possible prognostic implications.

REFERENCES

1. Marcus FI, McKenna WJ, Sherrill D, Basso C, Bauce B, Bluemke DA, Calkins H, Corrado D, Cox MGPJ, Daubert JP, Fontaine G, Gear K, Hauer R, Nava A, Picard MH, Protonotarios N, Saffitz JE, Sanborn DMY, Steinberg JS, Tandri H, Thiene G, Towbin JA, Tsatsopoulou A, Wichter T, Zareba W. Diagnosis of arrhythmogenic right ventricular cardiomyopathy/dysplasia: proposed modification of the task force criteria. Circulation 2010;121:1533–1541.
2. Corrado D, Link MS, Calkins H. Arrhythmogenic right ventricular cardiomyopathy. N Engl J Med 2017;376:61–72.
3. Cappelletto C, Stolfo D, De Luca A, Pinamonti B, Barbati G, Pivetta A, Gobbo M, Brun F, Merlo M, Sinagra G. Lifelong arrhythmic risk stratification in arrhythmogenic right ventricular cardiomyopathy: Distribution of events and impact of periodical reassessment. Europace 2018;20.
4. Saguner AM, Brunckhorst C, Duru F. Arrhythmogenic ventricular cardiomyopathy: A paradigm shift from right to biventricular disease. World J Cardiol 2014;6:154–174.
5. Corrado D, Zorzi A, Cipriani A, Bauce B, Bariani R, Beffagna G, De Lazzari M, Migliore F, Pilichou K, Rampazzo A, Rigato I, Rizzo S, Thiene G, Perazzolo Marra M, Basso C. Evolving diagnostic criteria for arrhythmogenic cardiomyopathy. J Am Heart Assoc 2021;10:e021987.
6. Pinamonti B, Dragos AM, Pyxaras SA, Merlo M, Pivetta A, Barbati G, Lenarda A Di, Morgera T, Mestroni L, Sinagra G. Prognostic predictors in arrhythmogenic right ventricular cardiomyopathy: results from a 10-year registry. Eur Heart J 2011;32:1105–1113.
7. Aquaro GD, De Luca A, Cappelletto C, Raimondi F, Bianco F, Botto N, Lesizza P, Grigoratos C, Minati M, Dell'Omodarme M, Pingitore A, Stolfo D, Dal Ferro M, Merlo M, Di Bella G, Sinagra G. Prognostic value of magnetic resonance phenotype in patients with arrhythmogenic Right ventricular cardiomyopathy. J Am Coll Cardiol 2020;75:2753–2765.
8. Miles C, Finocchiaro G, Papadakis M, Gray B, Westaby J, Ensam B, Basu J, Parry-Williams G, Papatheodorou E, Paterson C, Malhotra A, Robertus JL, Ware JS, Cook SA, Asimaki A, Witney A, Ster IC, Tome M, Sharma S, Behr ER, Sheppard MN. Sudden death and left ventricular involvement in arrhythmogenic cardiomyopathy. Circulation 2019;139:1786–1797.
9. Corrado D, Perazzolo Marra M, Zorzi A, Beffagna G, Cipriani A, De Lazzari M, Migliore F, Pilichou K, Rampazzo A, Rigato I, Rizzo S, Thiene G, Anastasakis A, Asimaki A, Bucciarelli-Ducci C, Haugaa KH, Marchlinski FE, Mazzanti A, McKenna WJ, Pantazis A, Pelliccia A, Schmied C, Sharma S, Wichter T, Bauce B, Basso C. Diagnosis of arrhythmogenic cardiomyopathy: The Padua criteria. Int J Cardiol 2020;319:106–114.

10. Borgquist R, Haugaa KH, Gilljam T, Bundgaard H, Hansen J, Eschen O, Jensen HK, Holst AG, Edvardsen T, Svendsen JH, Platonov PG. The diagnostic performance of imaging methods in ARVC using the 2010 Task Force criteria. Eur Hear journal Cardiovasc Imaging 2014;15:1219–1225.
11. Haugaa KH, Basso C, Badano LP, Bucciarelli-Ducci C, Cardim N, Gaemperli O, Galderisi M, Habib G, Knuuti J, Lancellotti P, McKenna W, Neglia D, Popescu BA, Edvardsen T. Comprehensive multi-modality imaging approach in arrhythmogenic cardiomyopathy-an expert consensus document of the European Association of Cardiovascular Imaging. Eur Hear journal Cardiovasc Imaging 2017;18:237–253.
12. Collier P, Phelan D, Klein A. A Test in Context: Myocardial strain measured by speckle-tracking echocardiography. J Am Coll Cardiol 2017;69:1043–1056.
13. Muser D, Castro SA, Santangeli P, Nucifora G. Clinical applications of feature-tracking cardiac magnetic resonance imaging. World J Cardiol 2018;10:210–221.
14. Sarvari SI, Haugaa KH, Anfinsen O-G, Leren TP, Smiseth OA, Kongsgaard E, Amlie JP, Edvardsen T. Right ventricular mechanical dispersion is related to malignant arrhythmias: a study of patients with arrhythmogenic right ventricular cardiomyopathy and subclinical right ventricular dysfunction. Eur Heart J 2011;32:1089–1096.
15. Prati G, Vitrella G, Allocca G, Muser D, Buttignoni SC, Piccoli G, Morocutti G, Delise P, Pinamonti B, Proclemer A, Sinagra G, Nucifora G. Right Ventricular strain and dyssynchrony assessment in arrhythmogenic right ventricular cardiomyopathy: cardiac magnetic resonance feature-tracking study. Circ Cardiovasc Imaging 2015;8:e003647; discussion e003647.
16. Pieles GE, Grosse-Wortmann L, Hader M, Fatah M, Chungsomprasong P, Slorach C, Hui W, Fan C-PS, Manlhiot C, Mertens L, Hamilton R, Friedberg MK. Association of echocardiographic parameters of right ventricular remodeling and myocardial performance with modified task force criteria in adolescents with arrhythmogenic right ventricular cardiomyopathy. Circ Cardiovasc Imaging 2019;12:e007693.
17. Mast TP, Taha K, Cramer MJ, Lumens J, Heijden JF van der, Bouma BJ, Berg MP van den, Asselbergs FW, Doevendans PA, Teske AJ. The prognostic value of right ventricular deformation imaging in early arrhythmogenic right ventricular cardiomyopathy. JACC Cardiovasc Imaging 2019;12:446–455.
18. Leren IS, Saberniak J, Haland TF, Edvardsen T, Haugaa KH. Combination of ECG and echocardiography for identification of arrhythmic events in early ARVC. JACC Cardiovasc Imaging 2017;10:503–513.
19. Shen M-T, Yang Z-G, Diao K-Y, Jiang L, Zhang Y, Liu X, Gao Y, Hu B-Y, Huang S, Guo Y-K. Left ventricular involvement in arrhythmogenic right ventricular dysplasia/cardiomyopathy predicts

adverse clinical outcomes: a cardiovascular magnetic resonance feature tracking study. Sci Rep 2019;9:14235.

20. Taha K, Bourfiss M, Riele ASJM Te, Cramer M-JM, Heijden JF van der, Asselbergs FW, Velthuis BK, Teske AJ. A head-to-head comparison of speckle tracking echocardiography and feature tracking cardiovascular magnetic resonance imaging in right ventricular deformation. Eur Hear journal Cardiovasc Imaging 2021;22:950–958.
21. Lang RM, Badano LP, Mor-Avi V, Afilalo J, Armstrong A, Ernande L, Flachskampf FA, Foster E, Goldstein SA, Kuznetsova T, Lancellotti P, Muraru D, Picard MH, Rietzschel ER, Rudski L, Spencer KT, Tsang W, Voigt J-U. Recommendations for cardiac chamber quantification by echocardiography in adults: an update from the American Society of Echocardiography and the European Association of Cardiovascular Imaging. J Am Soc Echocardiogr 2015;28:1-39.e14.
22. Nagueh SF, Smiseth OA, Appleton CP, Byrd BF 3rd, Dokainish H, Edvardsen T, Flachskampf FA, Gillebert TC, Klein AL, Lancellotti P, Marino P, Oh JK, Popescu BA, Waggoner AD. Recommendations for the evaluation of left ventricular diastolic function by echocardiography: an update from the american society of echocardiography and the European Association of Cardiovascular Imaging. J Am Soc Echocardiogr 2016;29:277–314.
23. Voigt J-U, Pedrizzetti G, Lysyansky P, Marwick TH, Houle H, Baumann R, Pedri S, Ito Y, Abe Y, Metz S, Song JH, Hamilton J, Sengupta PP, Kolias TJ, d'Hooge J, Aurigemma GP, Thomas JD, Badano LP. Definitions for a common standard for 2D speckle tracking echocardiography: consensus document of the EACVI/ASE/Industry Task Force to standardize deformation imaging. Eur Heart J Cardiovasc Imaging 2015;16:1–11.
24. Badano LP, Kolias TJ, Muraru D, Abraham TP, Aurigemma G, Edvardsen T, D'Hooge J, Donal E, Fraser AG, Marwick T, Mertens L, Popescu BA, Sengupta PP, Lancellotti P, Thomas JD, Voigt J-U. Standardization of left atrial, right ventricular, and right atrial deformation imaging using two-dimensional speckle tracking echocardiography: a consensus document of the EACVI/ASE/Industry Task Force to standardize deformation imaging. Eur Hear journal Cardiovasc Imaging 2018;19:591–600.
25. De Luca A, Stolfo D, Caiffa T, Korcova R, Barbati G, Vitrella G, Rakar S, Perkan A, Secoli G, Pinamonti B, Merlo M, Sinagra G. Prognostic value of global longitudinal strain-based left ventricular contractile reserve in candidates for percutaneous correction of functional mitral regurgitation: implications for patient selection. J Am Soc Echocardiogr 2019;32:1436–1443.
26. Merlo M, Masè M, Vitrella G, Belgrano M, Faganello G, Di Giusto F, Boscutti A, Gobbo M, Gigli M, Altinier A, Lesizza P, Barbati G, Ramani F, De Luca A, Morea G, Cova MA, Stolfo D, Sinagra G. Usefulness of addition of magnetic resonance imaging to echocardiographic imaging to predict

left ventricular reverse remodeling in patients with nonischemic cardiomyopathy. Am J Cardiol 2018;122:490–497.

27. Maceira AM, Prasad SK, Khan M, Pennell DJ. Normalized left ventricular systolic and diastolic function by steady state free precession cardiovascular magnetic resonance. J Cardiovasc Magn Reson 2006;8:417–426.
28. Aquaro GD, Todiere G, Strata E, Barison A, Bella G Di, Lombardi M. Usefulness of India ink artifact in steady-state free precession pulse sequences for detection and quantification of intramyocardial fat. J Magn Reson Imaging 2014;40:126–132.
29. Cerqueira MD, Weissman NJ, Dilsizian V, Jacobs AK, Kaul S, Laskey WK, Pennell DJ, Rumberger JA, Ryan T, Verani MS. Standardized myocardial segmentation and nomenclature for tomographic imaging of the heart. A statement for healthcare professionals from the Cardiac Imaging Committee of the Council on Clinical Cardiology of the American Heart Association. Int J Cardiovasc Imaging 2002;18:539–542.
30. Schulz-Menger J, Bluemke DA, Bremerich J, Flamm SD, Fogel MA, Friedrich MG, Kim RJ, Knobelsdorff-Brenkenhoff F von, Kramer CM, Pennell DJ, Plein S, Nagel E. Standardized image interpretation and post-processing in cardiovascular magnetic resonance - 2020 update : Society for Cardiovascular Magnetic Resonance (SCMR): Board of Trustees Task Force on Standardized Post-Processing. J Cardiovasc Magn Reson 2020;22:19.
31. Surkova E, Muraru D, Iliceto S, Badano LP. The use of multimodality cardiovascular imaging to assess right ventricular size and function. Int J Cardiol 2016;214:54–69.
32. Czimbalmos C, Csecs I, Dohy Z, Toth A, Suhai FI, Müssigbrodt A, Kiss O, Geller L, Merkely B, Vago H. Cardiac magnetic resonance based deformation imaging: role of feature tracking in athletes with suspected arrhythmogenic right ventricular cardiomyopathy. Int J Cardiovasc Imaging 2019;35:529–538.
33. Heermann P, Fritsch H, Koopmann M, Sporns P, Paul M, Heindel W, Schulze-Bahr E, Schülke C. Biventricular myocardial strain analysis using cardiac magnetic resonance feature tracking (CMR-FT) in patients with distinct types of right ventricular diseases comparing arrhythmogenic right ventricular cardiomyopathy (ARVC), right ventricular outflow-. Clin Res Cardiol 2019;108:1147–1162.
34. Chen X, Li L, Cheng H, Song Y, Ji K, Chen L, Han T, Lu M, Zhao S. Early left ventricular involvement detected by cardiovascular magnetic resonance feature tracking in arrhythmogenic right ventricular cardiomyopathy: the effects of left ventricular late gadolinium enhancement and right ventricular dysfunction. J Am Heart Assoc 2019;8:e012989.
35. Heermann P, Hedderich DM, Paul M, Schülke C, Kroeger JR, Baeßler B, Wichter T, Maintz D, Waltenberger J, Heindel W, Bunck AC. Biventricular myocardial strain analysis in patients with

arrhythmogenic right ventricular cardiomyopathy (ARVC) using cardiovascular magnetic resonance feature tracking. J Cardiovasc Magn Reson 2014;16:75.

36. Corrado D, Basso C. Arrhythmogenic left ventricular cardiomyopathy. Heart 2021;
37. Mast TP, Teske AJ, Heijden JF vd, Groeneweg JA, Riele ASJM Te, Velthuis BK, Hauer RNW, Doevendans PA, Cramer MJ. Left ventricular involvement in arrhythmogenic right ventricular dysplasia/cardiomyopathy assessed by echocardiography predicts adverse clinical outcome. J Am Soc Echocardiogr 2015;28:1103-13.e9.
38. Al-Jassar C, Bikker H, Overduin M, Chidgey M. Mechanistic basis of desmosome-targeted diseases. J Mol Biol 2013;425:4006–4022.
39. Perazzolo-Marra M, Leoni L, Bauce B, Corbetti F, Zorzi A, Migliore F, Silvano M, Rigato I, Tona F, Tarantini G, Cacciavillani L, Basso C, Buja G, Thiene G, Iliceto S, Corrado D. Imaging study of ventricular scar in arrhythmogenic right ventricular cardiomyopathy: comparison of 3D standard electroanatomical voltage mapping and contrast-enhanced cardiac magnetic resonance. Circ Arrhythm Electrophysiol 2012;5:91–100.
40. Zghaib T, Ghasabeh MA, Assis FR, Chrispin J, Keramati A, Misra S, Berger R, Calkins H, Kamel I, Nazarian S, Zimmerman S, Tandri H. Regional strain by cardiac magnetic resonance imaging improves detection of right ventricular scar compared with late gadolinium enhancement on a multimodality scar evaluation in patients with arrhythmogenic right ventricular cardiomyopathy. Circ Cardiovasc Imaging 2018;11:e007546.
41. Malik N, Win S, James CA, Kutty S, Mukherjee M, Gilotra NA, Tichnell C, Murray B, Agafonova J, Tandri H, Calkins H, Hays AG. Right ventricular strain predicts structural disease progression in patients with arrhythmogenic right ventricular cardiomyopathy. J Am Heart Assoc 2020;9:e015016.
42. Deshmukh T, Emerson P, Geenty P, Mahendran S, Stefani L, Hogg M, Brown P, Panicker S, Chong J, Altman M, Gottlieb D, Thomas L. The utility of strain imaging in the cardiac surveillance of bone marrow transplant patients. Heart 2021;
43. Alcidi GM, Esposito R, Evola V, Santoro C, Lembo M, Sorrentino R, Lo Iudice F, Borgia F, Novo G, Trimarco B, Lancellotti P, Galderisi M. Normal reference values of multilayer longitudinal strain according to age decades in a healthy population: A single-centre experience. Eur Hear journal Cardiovasc Imaging 2018;19:1390–1396.
44. Liu B, Dardeer AM, Moody WE, Hayer MK, Baig S, Price AM, Leyva F, Edwards NC, Steeds RP. Reference ranges for three-dimensional feature tracking cardiac magnetic resonance: comparison with two-dimensional methodology and relevance of age and gender. Int J Cardiovasc Imaging 2018;34:761–775.

45. Peng J, Zhao X, Zhao L, Fan Z, Wang Z, Chen H, Leng S, Allen J, Tan RS, Koh AS, Ma X, Lou M, Zhong L. Normal values of myocardial deformation assessed by cardiovascular magnetic resonance feature tracking in a healthy chinese population: a multicenter study. Front Physiol 2018;9:1181.

TABLES

Table 1. Main characteristics of the study population.

	All Patients 41	LONE RV AC 8 (20%)	BIVENTRICULAR AC 24 (58%)	LEFT-DOMINANT AC 9 (22%)	P
Age – years	44±13	40±11	49±13*	37±10*	**0.043**
Male – n (%)	26 (63)	7 (87)	14 (58)	5 (55)	0.286
2010 Task Force Criteria					
Global or regional dysfunction and structural alterations by imaging – Major criteria – n (%)	15 (37)	4 (50)†	11 (46)*	0 (0)* †	**0.035**
Global or regional dysfunction and structural alterations by imaging – Minor criteria – n (%)	11 (27)	2 (25)	7 (29)	2 (22)	0.915
ECG depolarization/conduction abnormalities – Major criteria – n (%)	2 (5)	1 (12)	1 (4)	0 (0)	0.474
ECG depolarization/conduction abnormalities – Minor criteria – n (%)	12 (29)	4 (50)†	8 (33)*	0 (0)*†	0.062
ECG repolarization abnormalities – Major criteria – n (%)	18 (44)	2 (25)	11 (46)	5 (56)	0.429
ECG repolarization abnormalities – Minor criteria – n (%)	10 (24)	0 (0)*	6 (25)	4 (44)*	0.103
Histology – Major criteria – n (%)	2 (5)	0 (0)	0 (0)*	2 (22)*	**0.024**
Histology – Minor criteria – n (%)	0 (0)	0 (0)	0 (0)	0 (0)	-
Arrhythmias – Major criteria – n (%)	16 (39)	3 (37)	9 (37)	4 (44)	0.931
Arrhythmias – Minor criteria – n (%)	22 (54)	4 (50)	13 (54)	5 (55)	0.971
Family history – Major criteria – n (%)	24 (58)	5 (62)	13 (54)	6 (67)	0.784
Family history – minor criteria – n (%)	2 (5)	0 (0)	0 (0)*	2 (22)*	**0.024**

Legend. AC=arrhythmogenic cardiomyopathy; ECG=Electrocardiogram; LV=left ventricle; RV=right ventricle; * † statistically significant.

Table 2. Baseline cardiac magnetic resonance parameters in the total population and according to AC phenotype.

	All Patients 41	LONE RV AC 8 (20%)	BIVENTRICULAR AC 24 (58%)	LEFT-DOMINANT AC 9 (22%)	P
LV EDVi – ml/m2	94±26	93±22	94±31	92±17	0.979
LVEF – %	54±10	59±6	53±12	51±8	0.244
LV WMA – n (%)	15 (34)	0 (0)*†	9 (37)*	6 (68)†	**0.017**
LV fat – n (%)	25 (57)	0 (0)*‡	21 (87)*†	4 (44)†‡	**<0.001**
LV fat extension – %	0.48 [0; 2.49]	0 [0; 0]*	1.61 [0.29; 2.91]*	0 [0; 2.67]	**0.002**
LV LGE – n (%)	27 (61)	0 (0)*†	18 (75)*	9 (100)†	**<0.001**
LV LGE extension – %	8.9 [1.05; 21]	0 [0; 0]* †	10 [3.47; 22.30]*	13.35 [8.60; 24.07]†	**<0.001**
RV EDVi – ml/m2	107±32	117±20*	113±35†	82±19*†	**0.034**
RVEF – %	49±12	47±9*	46±13†	59±5*†	**0.016**
RV WMA – n (%)	31 (70)	8 (100)*	23 (96)†	0 (0)*†	**<0.001**
RV fat – n (%)	24 (54)	5 (62)*	19 (79)†	0 (0)*†	**<0.001**
RV fat extension – %	2.18 [0; 5.41]	0.64 [0; 3.51]* †	4.33 [2.07; 10.85]* †‡	0 [0; 0] † ‡	**<0.001**
RV LGE – n (%)	14 (32)	1 (12)*‡	13 (54)†‡	0 (0)*†	**0.005**
RV LGE extension – %	0 [0 ; 6.92]	0 [0; 2.88]*	3.27 [0 ; 14.17]* ‡	0 [0; 0] ‡	**0.006**

Legend. AC=arrhythmogenic cardiomyopathy; EDVi=end-diastolic volume index; EF=ejection fraction; LGE=late gadolinium enhancement; LV=left ventricle; RV=right ventricle; WMA=wall motion abnormalities; * † ‡ statistically significant.

Table 3. Comparison of myocardial deformation indices between patients and healthy subjects. **a)** STE **b)** FT-CMR analysis.

Parameter	Patients n=41	Controls n=41	P
Age – years	44±13	39±12	0.068
Male – n (%)	26 (63)	25 (61)	0.500
ECHO LV GLS	-16.62±3.69	-21.28±2.72	**<0.001**
ECHO LV GCS	-16.13±4.66	-19.43±3.85	**0.002**
ECHO LV GRS	41.84±14.69	50.81±18.63	**0.029**
ECHO RV GLS	-16.70±5.63	-23.90±3.57	**<0.001**
ECHO RV FWLS	-16.88±6.37	-23.99±3.75	**<0.001**

Parameter	Patients n=41	Controls n=41	P
Age – years	44±13	34±10	**<0.001**
Male – n (%)	26 (63)	21 (51)	0.156
CMR LV 2DGLS	-17.10±3.22	-21.18±2.43	**<0.001**
CMR LV 3DGLS	-13.53±3.59	-16.73±2.22	**<0.001**
CMR LV 2DGCS	-17.73±6.61	-22.09±2.26	**<0.001**
CMR LV 3DGCS	-15.24±3.97	-18.96±2.27	**<0.001**
CMR LV 2DGRS	33.74±11.14	47.37±8.19	**<0.001**
CMR LV 3DGRS	32.42±11.17	45.58±11.35	**<0.001**
CMR RV 2DGLS	-19.85±6.46	-26.02±4.55	**<0.001**
CMR RV 2DGCS	-9.63±5.22	-15.51±3.29	**<0.001**
CMR RV 2DGRS	41.05±20.40	64.44±19.89	**<0.001**

Legend. CMR=cardiac magnetic resonance; ECHO=echocardiography; FWLS=free-wall longitudinal strain; GLS=global longitudinal strain; GCS= global circumferential strain; GRS= global radial strain; LV=left ventricle; RV=right ventricle.

Table 4. Myocardial deformation indices according to AC phenotype. **a)** STE **b)** FT-CMR analysis.

Parameter	All Patients 41	LONE RV AC 8 (20%)	BIVENTRICULAR AC 24 (58%)	LEFT-DOMINANT AC 9 (22%)	P
ECHO LV GLS	-16.62±3.69	-17.49±2.41	-16.43±4.08	-16.36±3.78	0.767
ECHO LV GCS	-16.13±4.66	-16.31±5.05	-16.48±4.34	-15.27±5.49	0.820
ECHO LV GRS	41.84±14.69	45.41±9.61	40.72±15.11	41.83±17.51	0.803
ECHO RV GLS	-16.70±5.63	-17.48±3.88	-14.72±5.48*	-21.29±4.76*	**0.007**
ECHO RV FWLS	-16.88±6.37	-16.82±4.96	-14.92±6.38*	-22.17±4.67*	**0.011**

Parameter	All Patients 41	LONE RV AC 8 (20%)	BIVENTRICULAR AC 24 (58%)	LEFT-DOMINANT AC 9 (22%)	P
CMR LV 2DGLS	-17.10±3.22	-17.17±2.63	-17.11±3.66	-16.99±2.69	0.993
CMR LV 3DGLS	-13.53±3.59	-15.07±2.35	-13.77±3.76	-11.53±3.45	0.112
CMR LV 2DGCS	-17.73±6.61	-19.36±3.13	-18.35±4.69	-14.61±4.45	0.059
CMR LV 3DGCS	-15.24±3.97	-16.34±2.65	-15.71±4.32	-13.00±3.36	0.149
CMR LV 2DGRS	33.74±11.14	38.04±9.23	35.04±11.76	26.44±8.03	0.064
CMR LV 3DGRS	32.42±11.17	33.91±7.17	34.37±12.49	25.89±8.35	0.139
CMR RV 2DGLS	-19.85±6.46	-20.94±4.02	-18.00±6.48	-23.83±6.68	0.057
CMR RV 2DGCS	-9.63±5.22	-8.59±4.33	-8.91±5.04	-12.47±4.84	0.180
CMR RV 2DGRS	41.05±20.40	44.22±9.44	33.91±19.67*	57.30±20.73*	**0.009**

Legend. CMR=cardiac magnetic resonance; ECHO=echocardiography; FWLS=free-wall longitudinal strain; GLS=global longitudinal strain; GCS= global circumferential strain; GRS= global radial strain; LGE=late gadolinium enhancement; LV=left ventricle; RV=right ventricle; * † ‡ statistically significant.

Table 5. Correlation between STE and FT-CMR analysis.

STE	FT-CMR	Spearman's Rho	P
LV GLS	LV 2DGLS	0.561	**<0.001**
	LV 3DGLS	0.662	**<0.001**
LV GCS	LV 2DGCS	0.332	0.105
	LV 3DGCS	0.284	0.169
LV GRS	LV 2DGRS	0.409	**0.042**
	LV 3DGRS	0.423	**0.035**
RV GLS	RV 2DGLS	0.310	0.084

Legend. CMR=cardiac magnetic resonance; FT=feature tracking; GLS=global longitudinal strain; GCS=global circumferential strain; GRS=global radial strain; LV=left ventricle; RV=right ventricle; STE=speckle tracking echocardiography.

Table 6. Correlation between STE and CMR parameters of biventricular involvement.

LV GLS

CMR Parameter	Spearman's Rho	P
LV wall motion score index	0.683	**<0.001**
LV fat extension - %	0.196	0.283
LV LGE extension - %	0.461	**0.008**

LV GCS

CMR Parameter	Spearman's Rho	P
LV wall motion score index	0.287	0.164
LV fat extension - %	0.095	0.652
LV LGE extension - %	0.304	0.140

LV GRS

CMR Parameter	Spearman's Rho	P
LV wall motion score index	-0.264	0.203
LV fat extension - %	-0.384	0.058
LV LGE extension - %	-0.335	0.101

RV GLS

CMR Parameter	Spearman's Rho	P
RV wall motion score index	0.706	**<0.001**
RV fat extension - %	0.433	**0.013**
RV LGE extension - %	0.506	**0.003**

RV FWLS

CMR Parameter	Spearman's Rho	P
RV wall motion score index	0.686	**<0.001**
RV fat extension - %	0.355	**0.046**
RV LGE extension - %	0.484	**0.005**

Legend. CMR=cardiac magnetic resonance; FWLS=free-wall longitudinal strain; GLS=global longitudinal strain; GCS=global circumferential strain; GRS=global radial strain; LGE=late gadolinium enhancement; LV=left ventricle; RV=right ventricle.

Table 7. Correlation between FT-CMR analysis and other CMR parameters of biventricular involvement.

2D LV GLS

CMR Parameter	Spearman's Rho	P
LV wall motion score index	0.664	**<0.001**
LV fat extension - %	0.053	0.773
LV LGE extension - %	0.262	0.098

3D LV GLS

CMR Parameter	Spearman's Rho	P
LV wall motion score index	0.722	**<0.01**
LV fat extension - %	0.258	0.154
LV LGE extension - %	0.423	**0.016**

2D LV GCS

CMR Parameter	Spearman's Rho	P
LV wall motion score index	0.698	**<0.001**
LV fat extension - %	0.160	0.382
LV LGE extension - %	0.388	**0.028**

3D LV GCS

CMR Parameter	Spearman's Rho	P
LV wall motion score index	0.702	**<0.001**
LV fat extension - %	0.057	0.755
LV LGE extension - %	0.362	**0.042**

2D LV GRS

CMR Parameter	Spearman's Rho	P
LV wall motion score index	-0.705	**<0.001**
LV fat extension - %	-0.164	0.370
LV LGE extension - %	-0.417	**0.018**

3D LV GRS

CMR Parameter	Spearman's Rho	P
LV wall motion score index	-0.661	**<0.001**
LV fat extension - %	-0.105	0.569
LV LGE extension - %	-0.396	**0.025**

RV GLS

CMR Parameter	Spearman's Rho	P
RV wall motion score index	0.435	**0.013**
RV fat extension - %	0.218	0.230
RV LGE extension - %	0.385	**0.030**

RV GCS

CMR Parameter	Spearman's Rho	P
RV wall motion score index	0.415	**0.018**
RV fat extension - %	0.173	0.344
RV LGE extension - %	0.450	**0.010**

RV GRS - LAX

CMR Parameter	Spearman's Rho	P
RV wall motion score index	-0.480	**0.005**
RV fat extension - %	-0.257	0.155
RV LGE extension - %	-0.459	**0.008**

Legend. CMR=cardiac magnetic resonance; GLS=global longitudinal strain; GCS=global circumferential strain; GRS=global radial strain; LAX=long axis; LGE=late gadolinium enhancement; LV=left ventricle; RV=right ventricle.

Table 8. Area under the ROC curves and proposed cut-off values of myocardial deformation indices for optimized sensitivity and specificity **a)** STE **b)** FT-CMR analysis.

Parameter	AUC	Cutoff	Sensitivity	Specificity
ECHO LV GLS	0.862	-20.35	0.85	0.71
ECHO LV GCS	0.714	-19.75	0.80	0.50
ECHO LV GRS	0.615	39.51	0.72	0.41
ECHO RV GLS	0.852	-20.45	0.78	0.83
ECHO RV FWLS	0.822	-20.05	0.73	0.87

Parameter	AUC	Cutoff	Sensitivity	Specificity
CMR LV 2DGLS	0.844	-19.92	0.81	0.71
CMR LV 3DGLS	0.772	-16.08	0.76	0.81
CMR LV 2DGCS	0.797	-21.16	0.73	0.70
CMR LV 3DGCS	0.778	-17.45	0.71	0.85
CMR LV 2DGRS	0.825	36.16	0.95	0.64
CMR LV 3DGRS	0.817	37.45	0.81	0.73
CMR RV 2DGLS	0.778	-24.60	0.83	0.68
CMR RV 2DGCS	0.839	-12.95	0.76	0.85
CMR RV 2DGRS	0.793	51.29	0.71	0.73

Legend. CMR=cardiac magnetic resonance; ECHO=echocardiography; FWLS=free-wall longitudinal strain; GLS=global longitudinal strain; GCS=global circumferential strain; GRS=global radial strain; LV=left ventricle; RV=right ventricle.

FIGURES

Central illustration. Imaging features of arrhythmogenic cardiomyopathy (AC). [1] Cardiac Magnetic Resonance (CMR) tissue characterization through Late Gadolinium Enhancement (LGE) technique in different AC phenotypes. (a-b) Lone right ventricular (RV) AC: marked RV dilatation with RV aneurysms and extensive LGE; (c-d) biventricular AC: aneurysm of RV free-wall and multiple areas of left ventricular (LV) LGE; (e-f) left-dominant AC: extensive LGE of inferior, posterior and lateral LV walls with epicardial distribution. [2] (a) Fat infiltration demonstrated by «India Ink» artifact in CMR balanced steady state free precession imaging confirmed by the detection of (b) hyperintense signal in proton-density-weighted black-blood turbo spin-echo images in the same anatomical location. [3] Analysis of RV strain through Speckle Tracking Echocardiography. [4] Analysis of biventricular strain through feature tracking CMR imaging.

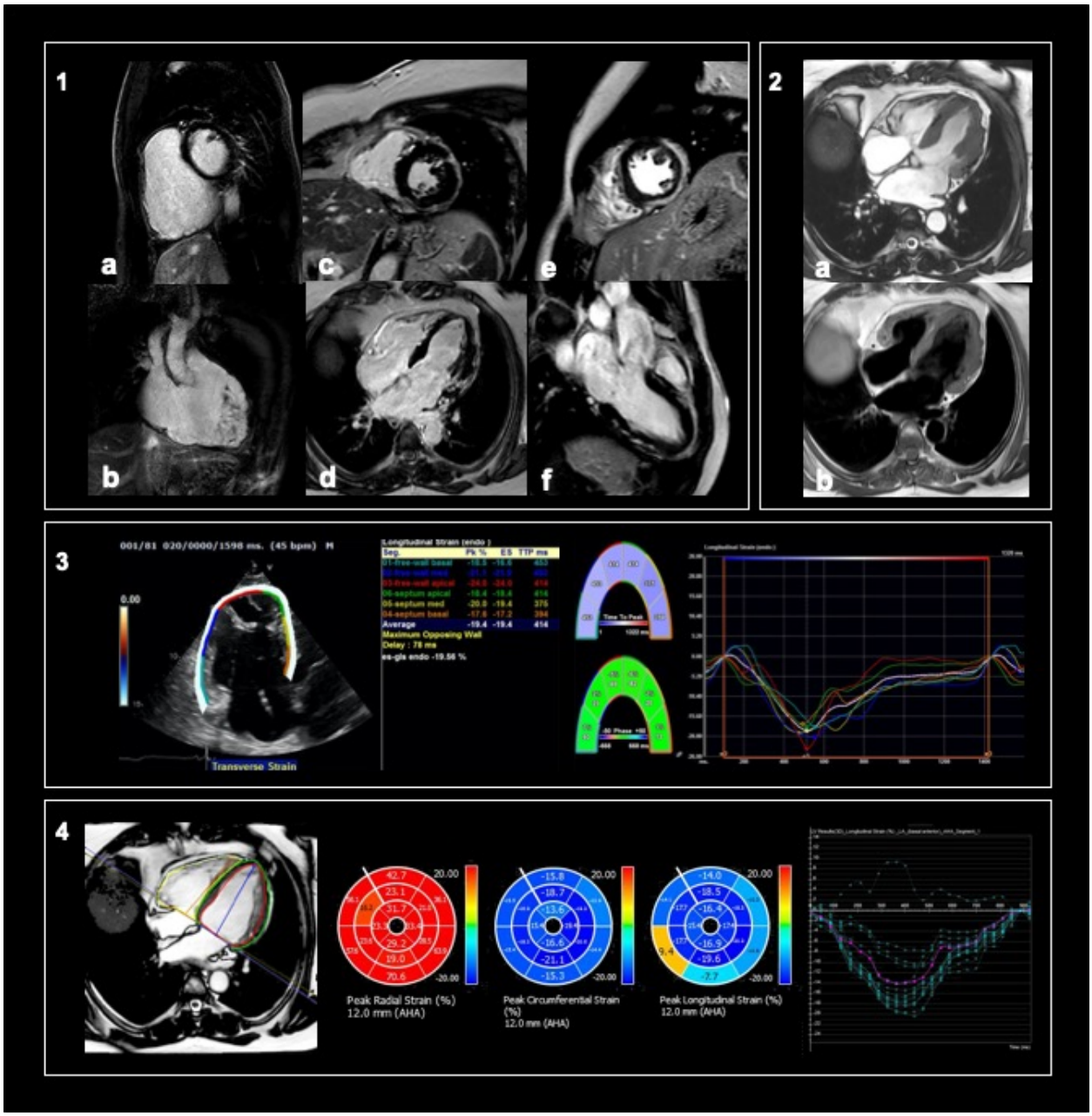

Figure 1. Scatter plots describing the correlation between LV GLS assessed by STE and FT-CMR analysis. A) correlation between echocardiographic LV GLS and CMR LV 2DGLS. B) correlation between echocardiographic LV GLS and CMR LV 3DGLS.

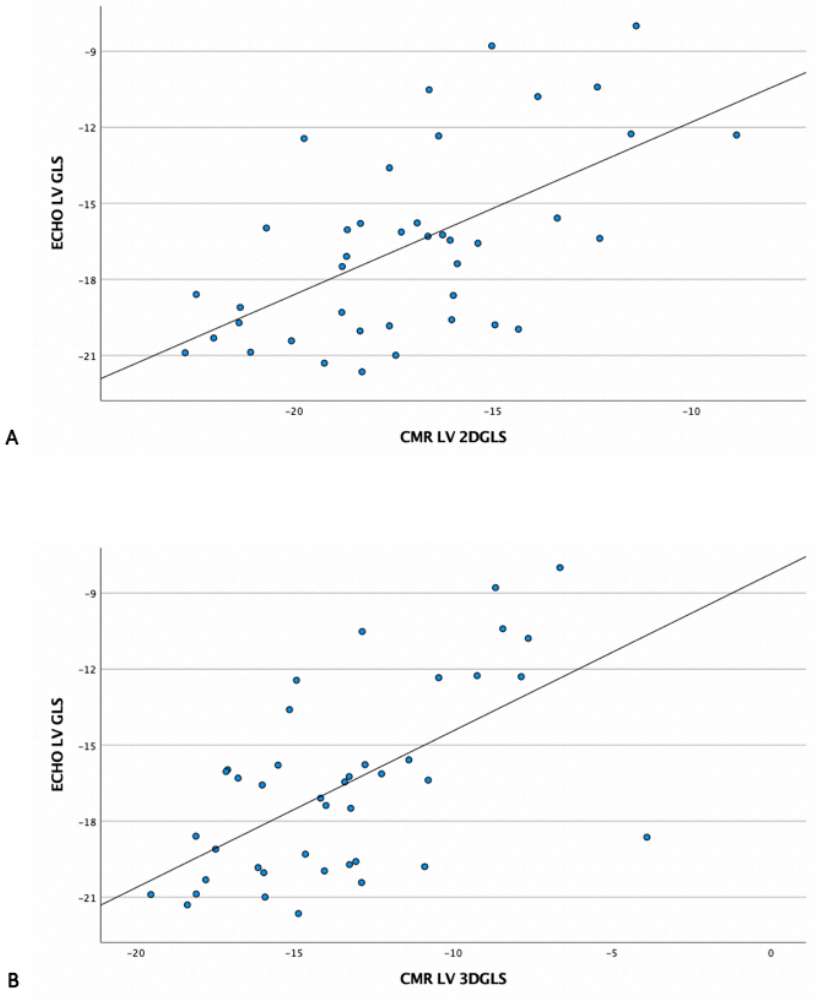

Legend. ECHO=echocardiography; CMR=cardiac magnetic resonance; FT=feature tracking; GLS=global longitudinal strain; LV=left ventricle; STE=speckle tracking echocardiography.

Figure 2. Scatter plots describing the correlation between LV GRS assessed by STE and FT-CMR analysis. A) correlation between echocardiographic LV GRS and CMR LV 2DGRS. B) correlation between echocardiographic LV GRS and CMR LV 3DGRS.

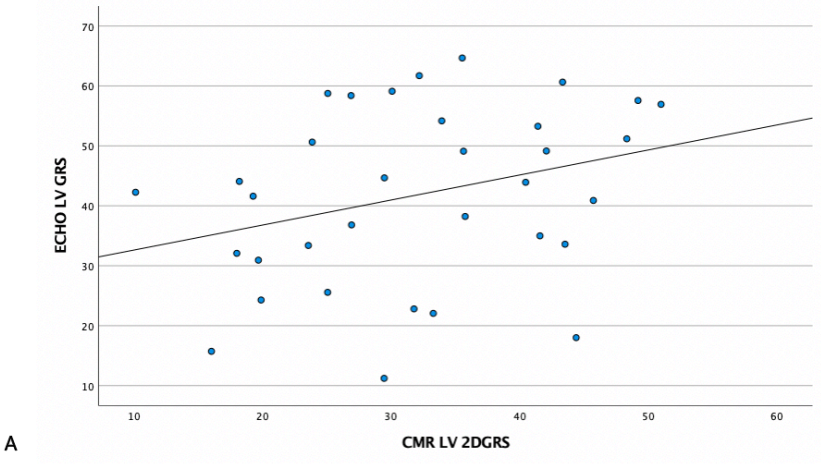

A

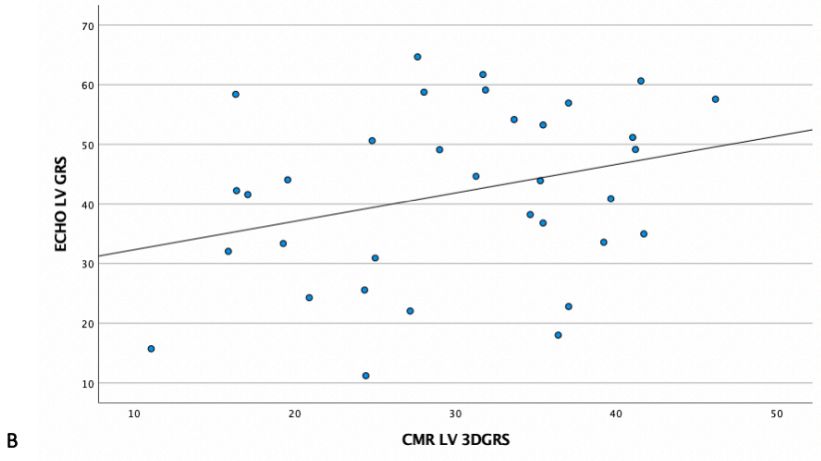

B

Legend. ECHO=echocardiography; CMR=cardiac magnetic resonance; GRS=global radial strain; LV=left ventricle.

Figure 3. Scatter plots describing the correlation between LGE extension expressed as percentage of LV myocardial mass and GLS assessed by A) STE and B-C) FT-CMR analysis.

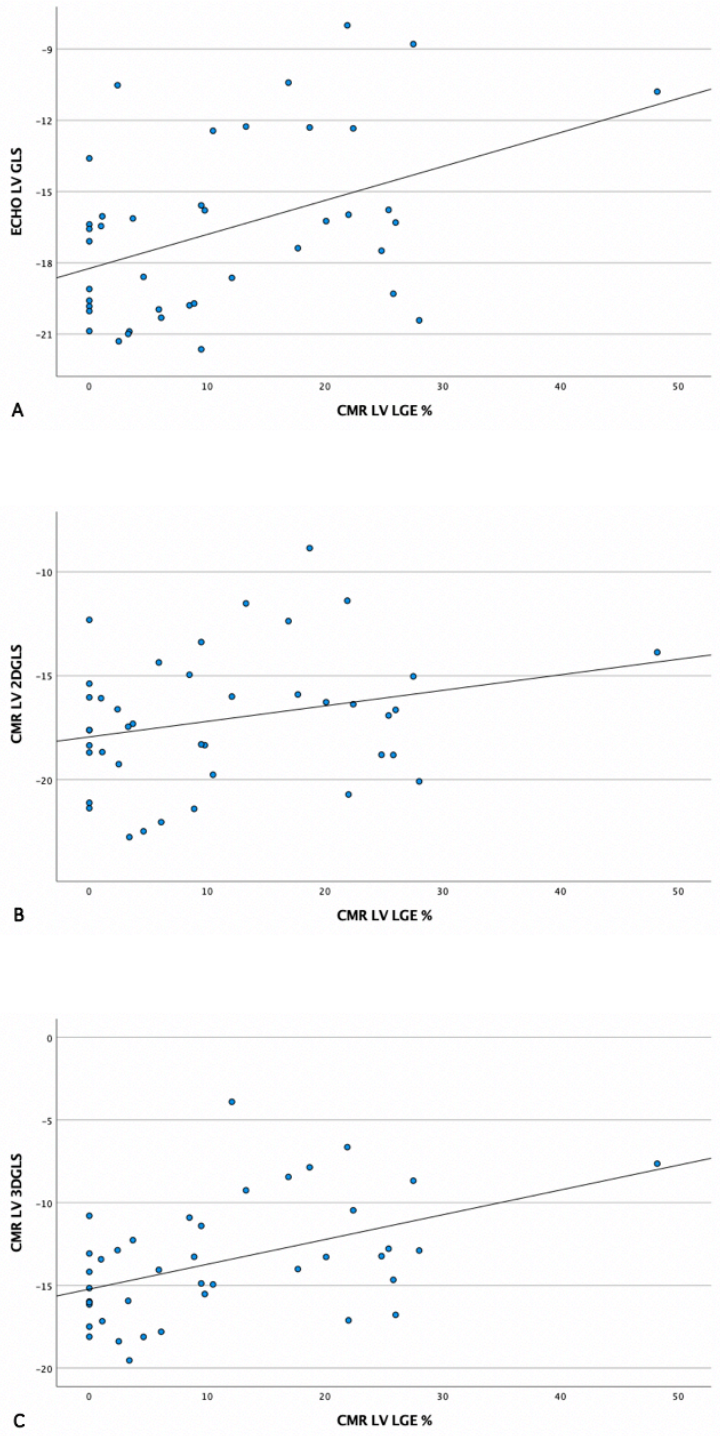

Legend. ECHO=echocardiography; CMR=cardiac magnetic resonance; FT=feature tracking; GLS=global longitudinal strain; LGE=late gadolinium enhancement; LV=left ventricle; STE=speckle tracking echocardiography.

Figure 4. Scatter plots describing the correlation between fat and LGE extension expressed as percentage of total RV myocardial area and RV GLS (A and B) and RV FWLS (C and D) assessed by STE.

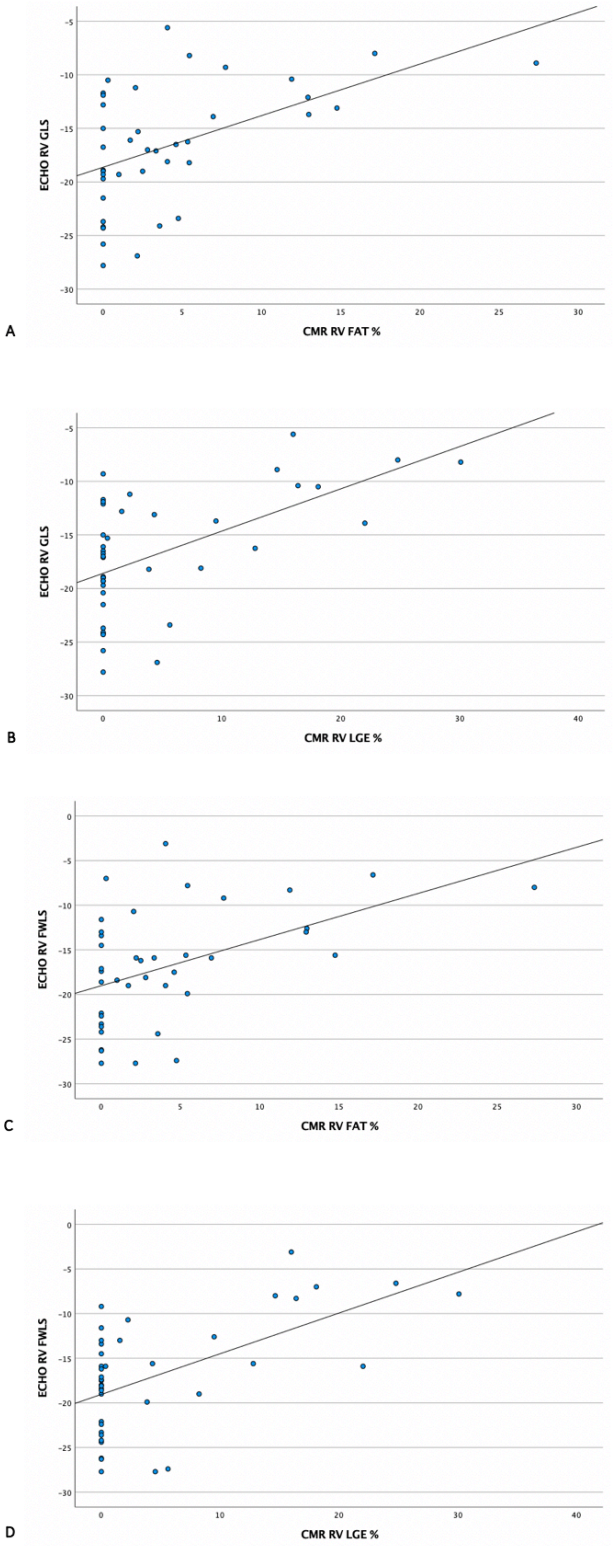

Legend. ECHO=echocardiography; CMR=cardiac magnetic resonance; GLS=global longitudinal strain; LGE=late gadolinium enhancement; RV=right ventricle.

Figure 5. Scatter plots describing the correlation between LGE extension expressed as percentage of LV myocardial mass and 2D (A and B) and 3D (C and D) GCS and GRS assessed by FT-CMR.

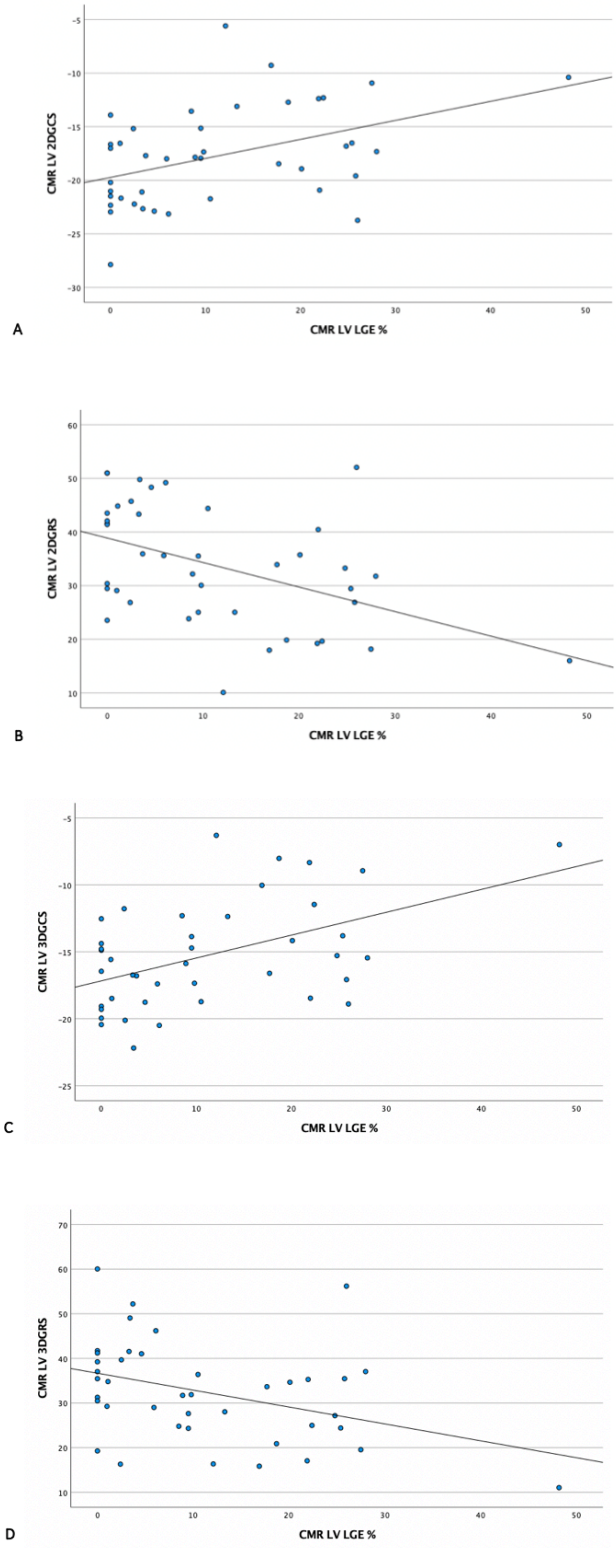

Legend. CMR=cardiac magnetic resonance; GLS=global longitudinal strain; GCS= global circumferential strain; GRS= global radial strain; LGE=late gadolinium enhancement; LV=left ventricle.

Figure 6. Scatter plots describing the correlation between LGE extension expressed as percentage of total RV myocardial area and deformation indices assessed by FT-CMR. A) CMR RV 2DGLS. B) CMR RV 2DGCS. C) CMR RV 2DGRS.

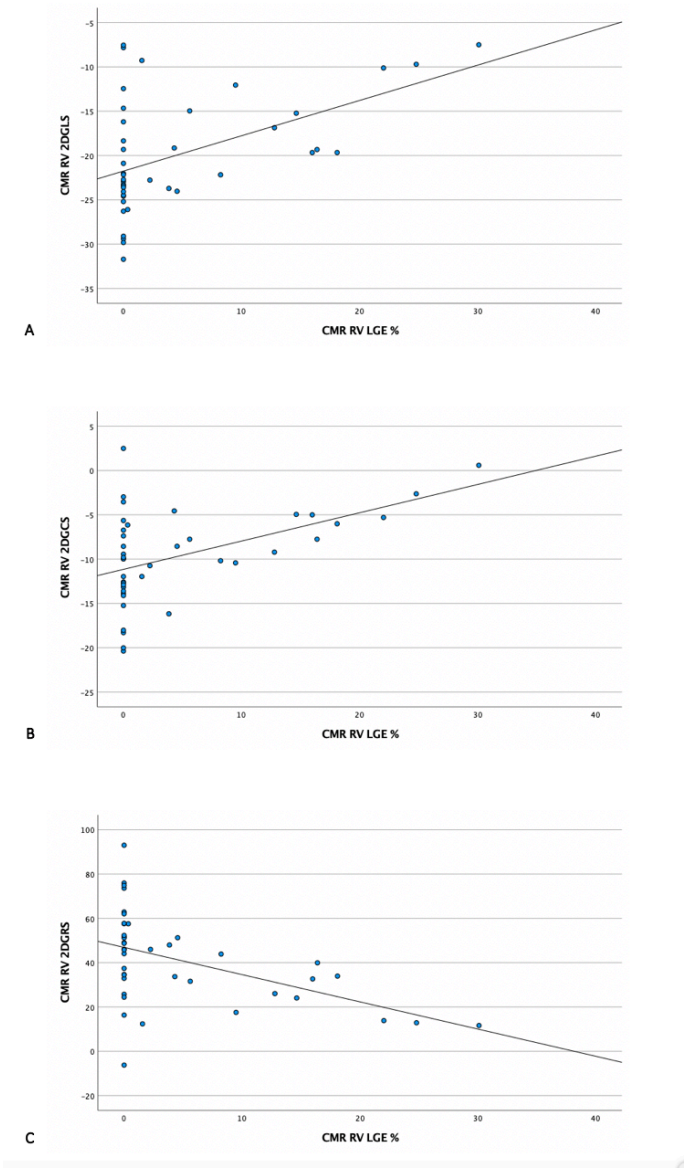

Legend. CMR=cardiac magnetic resonance; GLS=global longitudinal strain; LGE=late gadolinium enhancement; RV=right ventricle.

Figure 7. Receiver-operating characteristic (ROC) curves of echocardiographic myocardial deformation indices for differentiation of patients with AC from control subjects. AUC indicates area under the curve. LV strain analysis (A). RV strain analysis (B).

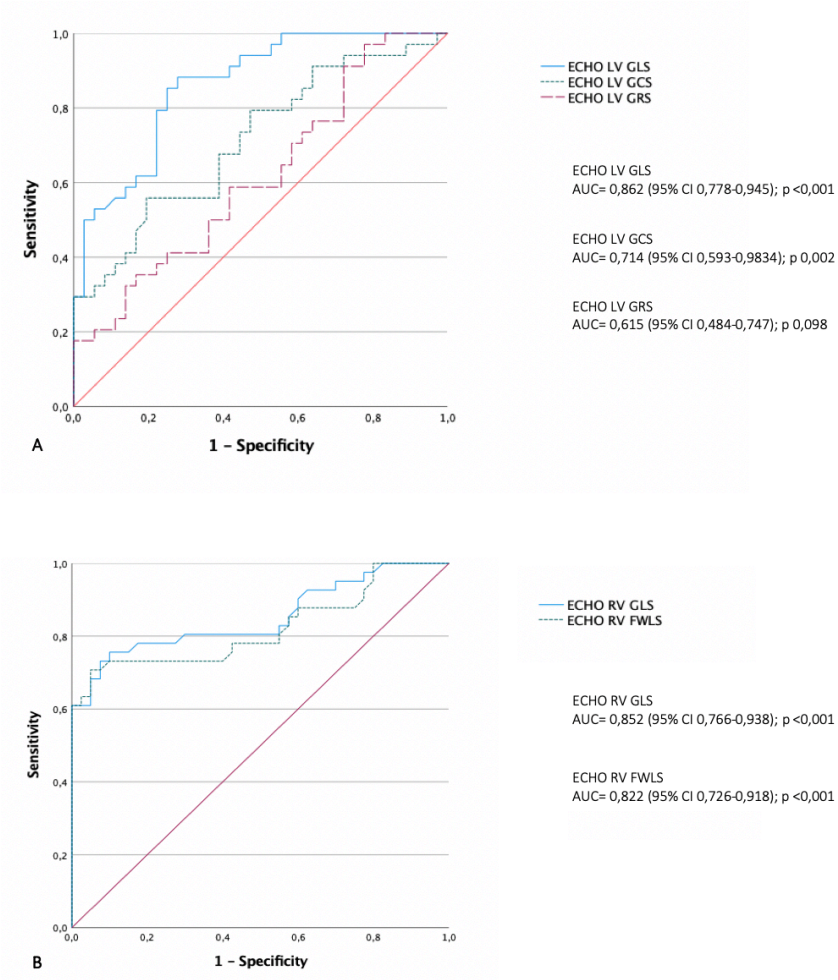

Legend. ECHO=echocardiography; FWLS=free-wall longitudinal strain; GLS=global longitudinal strain; GCS=global circumferential strain; GRS=global radial strain; LV=left ventricle; RV=right ventricle.

Figure 8. Receiver-operating characteristic curves of CMR myocardial deformation indices for differentiation of patients with AC from control subjects. AUC indicates area under the curve. LV 2D strain (A) LV 3D strain (B) RV 2D strain (C).

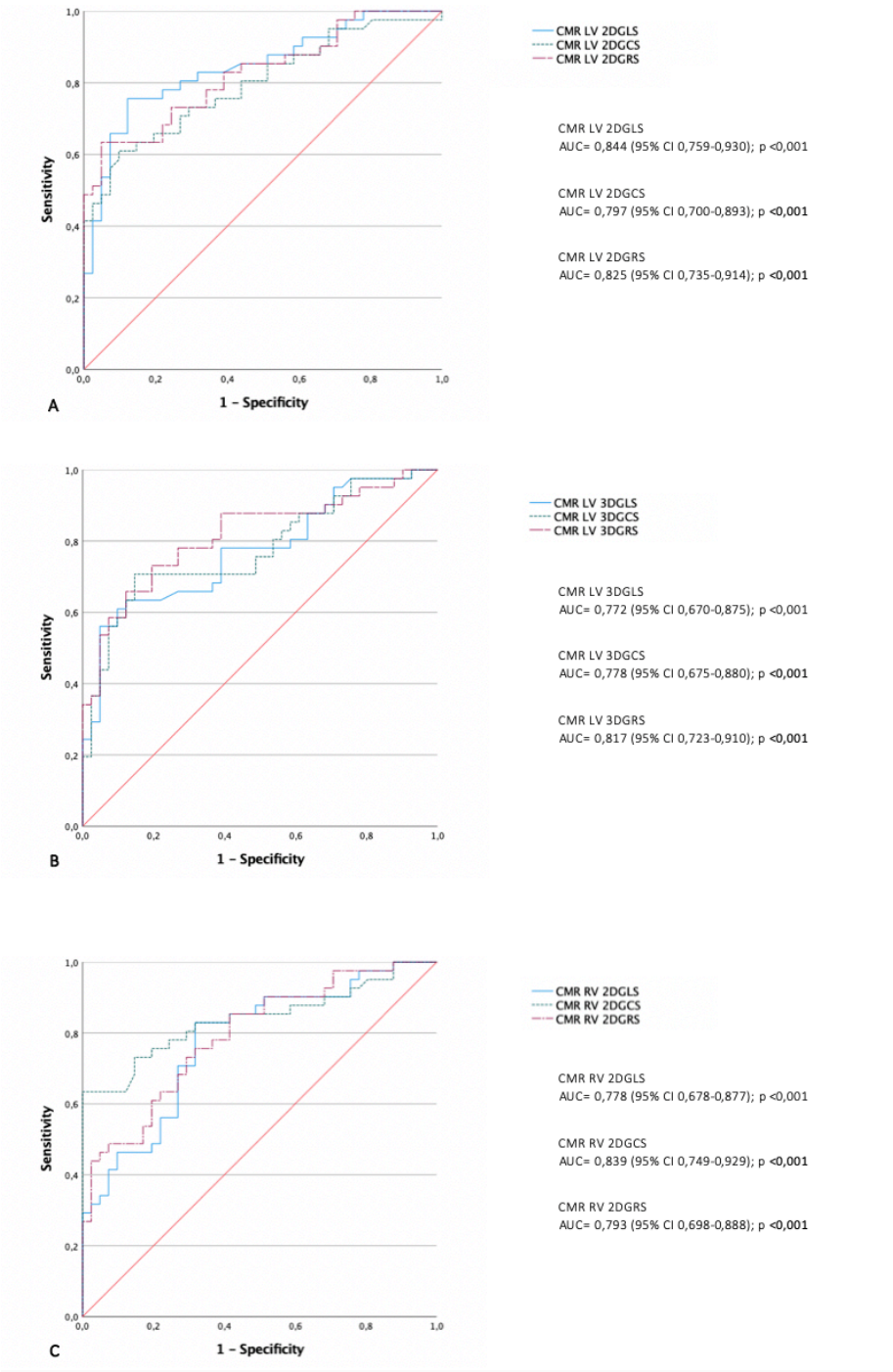

Legend. CMR=cardiac magnetic resonance; ECHO=echocardiography; GLS=global longitudinal strain; GCS=global circumferential strain; GRS=global radial strain; LV=left ventricle; RV=right ventricle.